

An Investigation of Tip-Vortex Turbulence Structure using Large-Eddy Simulation

¹David Hanson *; ¹Michael Kinzel; ¹Kyle Sinding; and ¹Michael Krane

¹The Pennsylvania State University, University Park, PA, USA

Abstract

In this effort, the tip vortex behind a rectangular plan-form lifting fin with a cavitation-relevant airfoil section (NACA-66 mod) is studied using Large Eddy Simulation (LES) at a free-stream Reynolds number of 500,000. Elementary flow quantities (lift, drag, velocities) are compared with measurements made in the Garfield Thomas Water Tunnel (GTWT) 12-inch circular test-section. Good agreement is seen with the measured lift and drag. The characteristic 45-degree lag between the mean strain rate and the Reynolds stress components in the plane of the tip vortex is observed. The calculated flow field provides insight into the turbulent structure of the tip vortex for this fin.

Keywords: tip-vortex, turbulence, computational fluid dynamics

Introduction

Cavitation within tip-vortices, *i.e.*, Tip-Vortex Cavitation (TVC), is important aspect relevant to the design of propellers for underwater vehicles [1]. One specific adverse aspect is erosion associated when a cavitating vortex impacts downstream surfaces. Understanding the complicated turbulent flow-field in the region of TVC inception is necessary in order to develop Computational Fluid Dynamics (CFD) models to predict TVC.

In the present literature, the authors found a limited database of detailed turbulent structure information within tip vortices. The turbulence, however, directly informs the overall tip-vortex evolution and the development of TVC. The cavitation behavior within a tip vortex is informed by the turbulent pressure and velocity fluctuations. The challenges involved in measuring experimentally both the time-varying pressure and velocity fields within a tip vortex are considerable. As such, the established understanding of the correlation between these quantities is limited. The present work involves a numerical study using Large-Eddy Simulation (LES) of a tip-vortex flow around a rectangular fin to gain detailed insight into the resulting turbulent flow-field. The tip-vortex flow geometry in question was recently studied experimentally by Sinding and Krane [2].

For the present work, the authors will interrogate the unsteady LES flow-field solution to extract the fine details of the turbulent structure. LES will, thus, be used to develop a thorough understanding of Reynolds-Averaged Navier-Stokes (RANS) turbulence model failure in tip-vortex flows.

Description of the Flow

The fin geometry considered in this work was studied experimentally by Sinding and Krane [2]. The chord is 4in (0.1016m) and the aspect ratio is two. The fin has an NACA-66(mod) thickness distribution [3] wrapped around an NACA 4-digit camber line. The maximum camber in the chord-wise direction is $0.0192 \times \text{chord}$, located at 50% chord. The camber is uniform along the span and was chosen such that at zero incidence the lift coefficient is 0.4 with a span-wise lift distribution that is approximately elliptical. A similar fin was also studied experimentally by Hanson [4]; however, the fin at that time had a geometry with a rounded tip. Sinding and Krane modified the fin model to have a flat tip in order to simplify the boundary-layer detachment as the flow enters the tip vortex. Because the shape of the fin tip is expected to influence strongly the tip-vortex dynamics, this paper focuses only on the flat-tipped fin studied by Sinding and Krane. The physical fin model is shown in the 12-inch (0.3048m) circular test-section water tunnel at Penn State's Applied Research Laboratory in Figure 1.

The present computational model includes the fin geometry and the circular water tunnel section. The free-stream speed is $15 \frac{\text{ft}}{\text{s}}$ ($4.57 \frac{\text{m}}{\text{s}}$), yielding a moderate Reynolds number of $\sim 5 \times 10^5$. The tunnel is modeled in order for the calculated lift and drag to be directly comparable with the experimental measurements without correcting for the

*Corresponding Author, David Hanson: drh5013@psu.edu

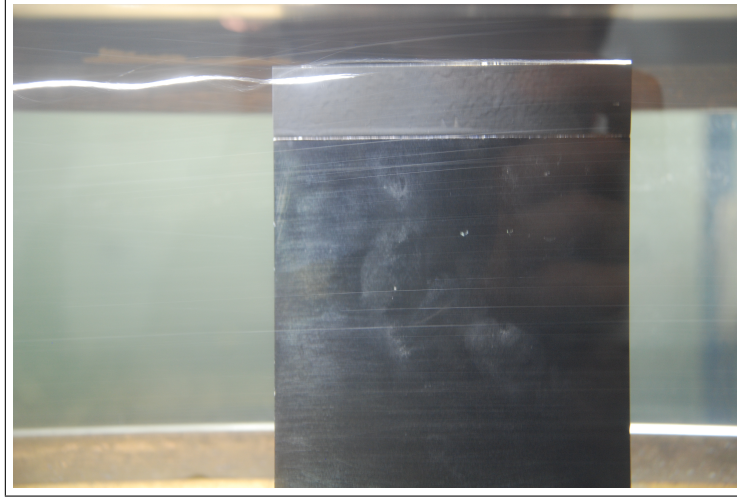


Figure 1: Side view of the fin in the water tunnel. TVC is visible near the top of the figure downstream of the tip. Flow is right-to-left.

blockage or the presence of walls. The present work uses a geometry and computational mesh as corresponding to that presented in Figure 2.

Methods

Flow Solver

In the present work, the discretized LES equations of fluid motion are solved in the context of the commercial CFD suite Star-CCM+ [5]. Star-CCM+ is developed and maintained by CD-Adapco, a division of Siemens Corporation. Star-CCM+ is capable of many different spatial and temporal solution methods; only those relevant to the present work are discussed here.

The spatial- and temporal-discretization schemes used are formally second-order accurate. Pressure-velocity coupling in the present incompressible flow is accomplished at each time step in a segregated manner via the SIMPLE algorithm, wherein a discrete pressure-Poisson equation provides an update to the solution of the discretized momentum conservation equations within each linear sub-iteration. All solution variables are located at the cell centers; facial fluxes are approximated via a Total-Variation Bounding (TVB) central-difference scheme.

Equations of Fluid Motion

The subgrid-filtered equations of mass- and momentum-conservation for LES of an incompressible flow are written as

$$\frac{\partial \bar{u}_j}{\partial x_j} = 0 \quad (1)$$

and

$$\frac{\partial \bar{u}_i}{\partial t} + \frac{\partial}{\partial x_j} (\bar{u}_i \bar{u}_j + \delta_{ij} \bar{p} - \bar{\mathcal{T}}_{ij}) = \frac{\partial \tau_{ij}^r}{\partial x_j} \quad (2)$$

where the overline in this context refers to variables that have undergone the subgrid filter.

Formally, the residual stress tensor $\tau_{ij}^r = \overline{u_i u_j} - \bar{u}_i \bar{u}_j$ represents contributions from three types of interactions: interactions among resolved scales, interactions among the unresolved scales, and cross-interactions between resolved and unresolved scales. These are typically called the Leonard stress, the Reynolds stress, and the Clark stress, respectively. In practice, however, this term is modeled via a Boussinesq approximation, $\tau_{ij}^r =$

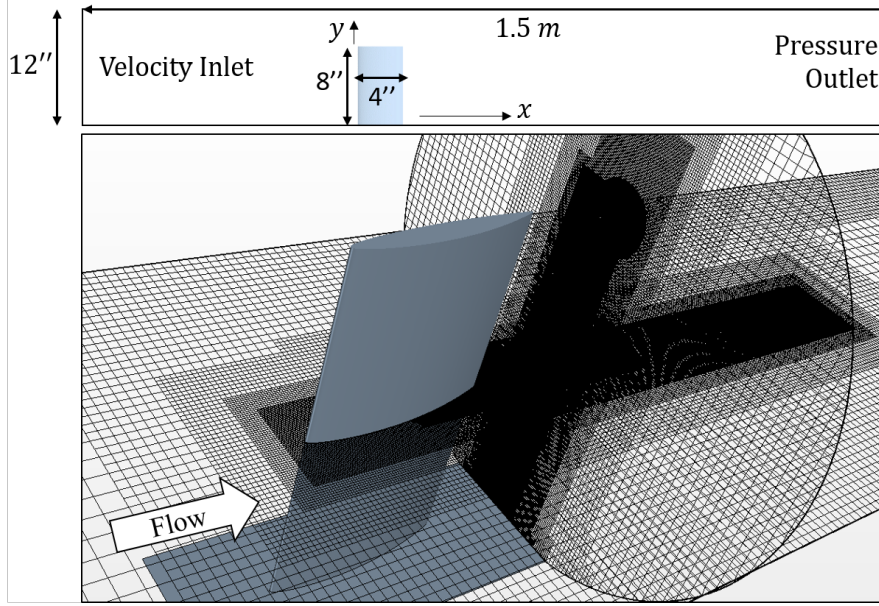


Figure 2: *Top*: geometry of the flow over the finite-span fin in the 12in (0.3048m) circular test section of the water-tunnel. The z -direction points into the page and completes the right-handed set. The origin is coincident with where the fin leading edge meets the tunnel wall. *Bottom*: the refinement regions overlaid upon the fin geometry.

$2(\nu_{t,SGS}S_{ij} - \delta_{ij}k_{SGS}/3)$, where k_{SGS} is the subgrid-scale turbulent kinetic energy. The subgrid turbulent viscosity, $\nu_{t,SGS}$, is given by a simple function evaluation in terms of the local strain rate and the mesh size. The Wall-Adapting Large Eddy (WALE) constitutive model is used to define $\nu_{t,SGS}$ in the present work [6].

Discretization

The flow equations of motion are discretized and solved on an unstructured trimmed Cartesian mesh with prism layers. This mesh type was chosen because it allows the best compromise between the competing goals of minimizing the numerical dissipation, minimizing the total cell count required to resolve the geometry, and minimizing the mesh generation time. Within the high-resolution turbulence-resolving region, the mesh is uniform and rectilinear with the exception of the thin near-wall prism layer. Such a uniform mesh reduces the importance of numerical diffusion and errors due to the gradient reconstruction.

The computational mesh used in the present study has approximately 70×10^6 cells. As mentioned by Georgiadis *et al.* [7], the spatial resolution of the mesh used for LES is typically determined by the maximum limit of the computing resources available. That is also the case here. Rather than resolving the viscous sublayer, the lowest region of the boundary layer at the surface of the fin is approximated using a blended wall function based on Reichardt's law. The dimensionless distance, $y^+ = \Delta y u^*/\nu$, from the wall to the nearest cell center, is between 20 and 100 on the fin surface. In outer variables, this yields a wall-normal cell size of $\Delta y/\delta \approx 0.02$, consistent with the recommendation of Larsson *et al.* [8] for LES. Because this is a relatively simple wing geometry, without strong pressure gradients or separated flow regions, use of wall functions is not expected to be detrimental to the solution quality. The linear size of wall cells in the wall-parallel direction is 0.25 mm, or $x^+, z^+ \sim 50$. The near-wall region of mesh refinement is shown in Figure 2. The present mesh provides approximately 40 grid points across the vortex core diameter within the region of highest refinement. Using the computed solution, the Taylor microscale (λ) is approximated and compared to the computational cell size in the Results section.

The time step is chosen such that the convective Courant number is less than unity in almost all computational cells. For the present flow, a time step of 25 microseconds satisfies this requirement. Ten linear iterations are performed within each non-linear time step. The solution was run for a total simulation time of 0.55 seconds; this corresponds to a simulation time of approximately 24 convective time scales. Time-averages for the various

P	$-\overline{u'_j u'_k \frac{\partial \bar{u}_j}{\partial x_i}} - \overline{u'_i u'_j \frac{\partial \bar{u}_k}{\partial x_i}}$	P_{TKE}	$-\overline{u'_i u'_j \frac{\partial \bar{u}_j}{\partial x_i}}$
DS	$-2\nu \frac{\partial u'_k}{\partial x_i} \frac{\partial u'_i}{\partial x_j}$	ϵ	$\nu s'_{ij} s'_{ij}$
PSC	$\frac{p'}{\rho} \left(\frac{\partial u'_j}{\partial x_k} + \frac{\partial u'_k}{\partial x_j} \right)$	$DF_{TKE,1,pressure}$	$\frac{\partial}{\partial x_i} \left(-\overline{u'_i p'} \right)$
DF_1	$\frac{\partial}{\partial x_i} \left(-\overline{u'_i u'_j u'_k} \right)$	$DF_{TKE,1}$	$\frac{\partial}{\partial x_i} \left(-\overline{u'_i u'_j u'_j} \right)$
DF_2	$\nu \frac{\partial^2}{\partial x_i \partial x_i} \left(\overline{u'_j u'_k} \right)$	$DF_{TKE,2}$	$\nu \frac{\partial^2 k}{\partial x_i \partial x_i}$
DF_3	$\frac{\partial}{\partial x_i} \left(-\frac{p'}{\rho} \left(\delta_{ij} u'_k + \delta_{ik} u'_j \right) \right)$	$DF_{TKE,3}$	$\nu \frac{\partial^2}{\partial x_i \partial x_i} \left(\overline{u'_j u'_j} \right)$

Table 1: Meaning of terms in RS equation (left) and the TKE equation (right)

quantities discussed in the Results section were recorded for approximately the last quarter second, or half the total simulation time, in order to avoid contaminating the averages with flow transients.

Turbulence Quantities

A goal of this study is to provide quantitative information regarding the detailed turbulent structure within the tip vortex as it undergoes the wrap-up process. Toward this end, every term both in the Reynolds Stress (RS) equation and in the much simpler Turbulent Kinetic Energy (TKE) equation is recorded at every fourth time step on two planes (at one-quarter and one chord downstream of the trailing edge) across the tip vortex. Furthermore, time-averaged values of every term in the TKE equation are recorded at every cell in the domain.

In the context of a Cartesian coordinate system, the transport equation for each component of the RS tensor for an incompressible Newtonian flow is:

$$\frac{\partial}{\partial t} \left(\overline{u'_j u'_k} \right) + \bar{u}_i \frac{\partial}{\partial x_i} \left(\overline{u'_j u'_k} \right) = P_{RS} + DS_{RS} + PSC_{RS} + DF_{RS,1} + DF_{RS,2} + DF_{RS,3} \quad (3)$$

where the symbols on the right side of the equation represent tensors that express turbulence production, pseudo-dissipation, the correlation between pressure and strain, and three types of diffusion, respectively. The forms for these terms used in the present work are summarized in Table 1. Each term in this table is a symmetric second order tensor and therefore has six independent components that must be recorded.

A common simplification of the RS tensor equation is to assume that the dynamics of turbulence is controlled by the trace of the RS tensor, interpreted as the TKE, $k = \frac{1}{2} \left(\overline{u'^2} + \overline{v'^2} + \overline{w'^2} \right)$. This reduces the six tensor RS equations to a scalar equation for k :

$$\frac{\partial k}{\partial t} + \bar{u}_i \frac{\partial k}{\partial x_i} = P_{TKE} - \epsilon + DF_{TKE,1,pressure} + DF_{TKE,1} + DF_{TKE,2} + DF_{TKE,3} \quad (4)$$

where the right-hand-side symbols represent turbulence production, dissipation, and four types of diffusion, respectively. These are also summarized in Table 1.

The approach taken for the present work is to track the instantaneous and mean values of the five field variables for the TKE equation and the instantaneous values for the further 36 variables for the RS equation. This is in addition to seven field variables for RS and TKE. All instantaneous variables in the RS equation were exported every fourth time step on two planes normal to the tip vortex located $0.25 \times \text{chord}$ and $1 \times \text{chord}$ downstream of the trailing edge, respectively; time-averaged quantities for the RS equation are therefore available only on these planes.

Results

Validation

The lift- and drag-coefficients, *i.e.*, C_L and C_D , respectively, computed for the present flow are compared with experimental measurements made by Hanson for this fin [4] in Figure 3. Recall that the fin used in those experi-

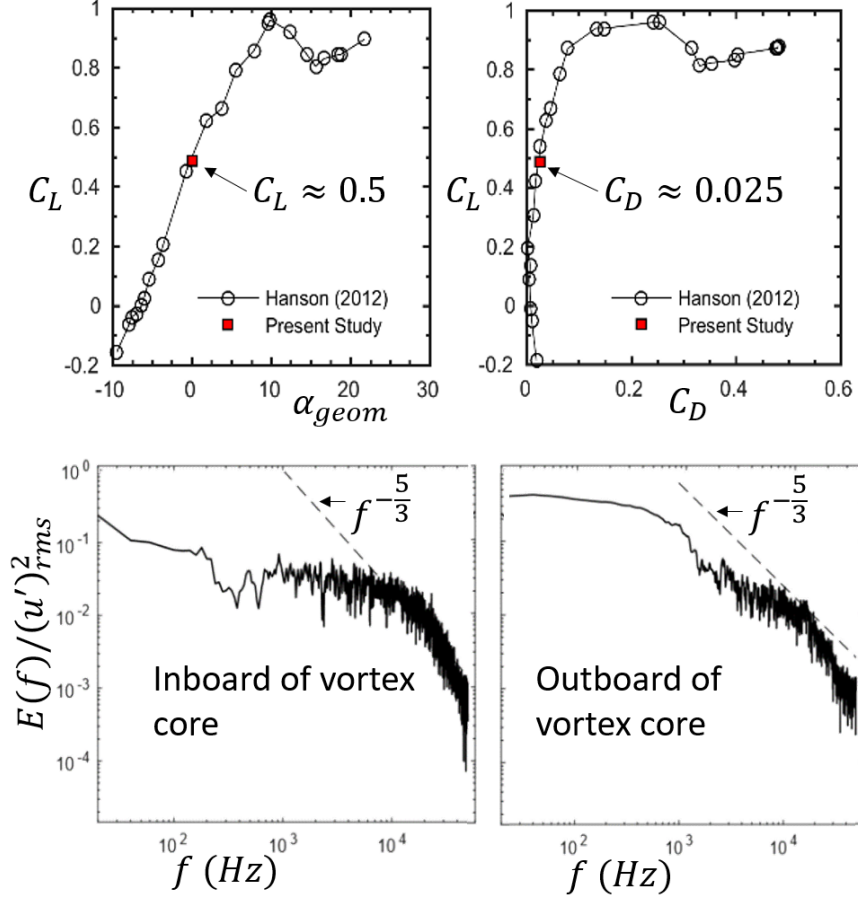


Figure 3: *Top Row:* C_L from the present study compared with the measurements of Hanson [4]. C_D measurements from that study are compared with the present CFD in the rightmost figure. *Bottom Row:* spectra of turbulent velocity fluctuations at two locations in the flow: immediately inboard (left) and outboard (right) of the vortex core; both probes are located one inch downstream of the trailing edge. The specific kinetic energy in the flow, $E = \frac{1}{2}u^2$, is made dimensionless by the local velocity variance, $(u'^2)_{rms}$.

mental measurements had a rounded, rather than CFD model having a flat-tip geometry. It is not anticipated that the tip geometry greatly to alter C_L and C_D . Agreement between the present CFD and experimental measurements is quite close.

TKE spectra are shown for two different point probes within the tip vortex in Figure 3. The velocity point probes are located on the inboard and outboard edges of the tip vortex, respectively, $1in$ ($0.0254m$) downstream of the trailing edge. The expected $f^{-5/3}$ decay of the kinetic energy with respect to frequency is observed at higher frequencies at both locations.

In the present work, λ is approximated from the flow solution as $\lambda \sim \sqrt{10\nu k/\epsilon}$. The ratio of this length scale to the computational cell linear size, h , is shown in Figure 4 on a planar slice through the tip vortex at an axial location one chord downstream of the trailing edge. It is seen that the present mesh has approximately five cells per λ within the wake and at the edge of the vortex core.

Elementary Turbulence Quantities

For the sake of brevity, only one elementary turbulence quantity is mentioned here. The rightmost image in Figure 4 compares the $y - z$ component of the mean strain rate tensor, S_{ij} , with the corresponding component of the specific Reynolds stress tensor τ_{ij} . Chow [9] observed that the Reynolds shear stress in the plane of the tip vortex

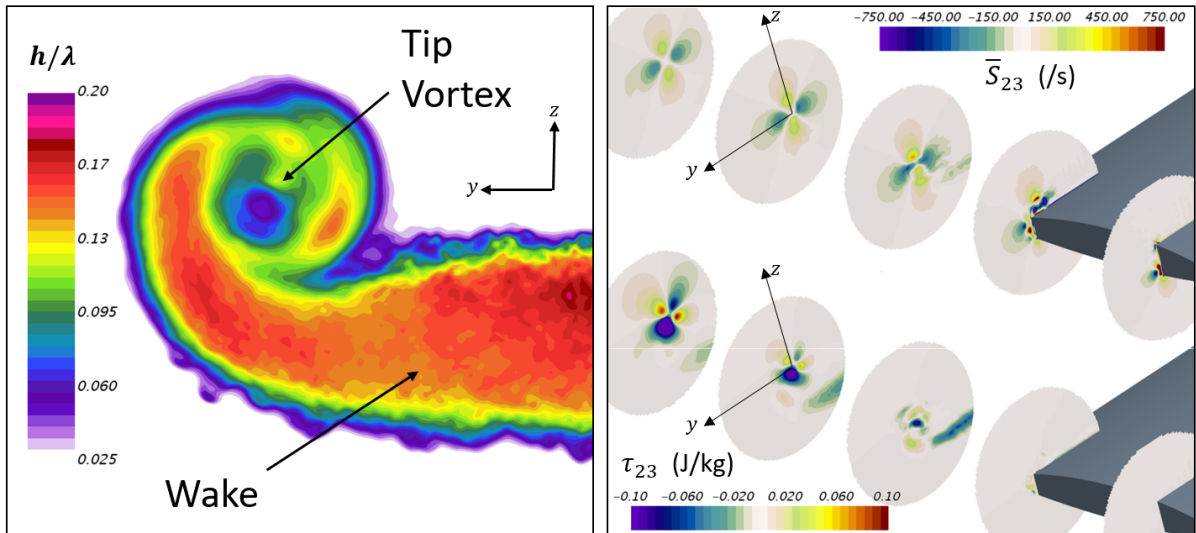


Figure 4: *Left*: ratio of the cell linear size, h , to the approximate λ . *Right*: comparison of the mean shear rate component \bar{S}_{23} with the corresponding Reynolds stress component τ_{23} .

tends to lag the corresponding component of the mean strain rate by 45° . It is worth noting that RANS turbulence models that use a linear Boussinesq closure expression are unable to produce Reynolds stresses that are not aligned with the mean strain rate. Several authors (see, for example, Churchfield and Blaisdell [10]) have proposed that this weakness in the linear Boussinesq approximation makes a key contribution to RANS models diffusing tip vortices much more quickly than is seen in experiments. The present simulation shows the expected 45° offset between the lobes of \bar{S}_{23} and τ_{23} once the vortex rollup is complete approximately one chord downstream of the trailing edge.

Future Work

The remaining terms in the TKE equation are to be extracted from the flow solution and explored in detail. This will include determining the dominant terms in the turbulent energy budget as the vortex evolves downstream of the trailing edge.

Furthermore, the pressure variance, $(p')^2_{rms}$ will be compared with a common approximate expression for the pressure fluctuations, $p' \sim 0.39\rho k$. This approximation is appropriate for isotropic, homogeneous turbulence; however, it will be seen that it does not adequately capture the character of the turbulent pressure fluctuations within the highly ordered, anisotropic vortex core. This has implications for RANS-based cavitation models.

References

- [1] Barnes W McCormick, Jr. *A Study of the Minimum Pressure in a Trailing Vortex System*. Doctoral dissertation, Pennsylvania State University, 1954.
- [2] K Sinding and M Krane. Tip vortex core pressure estimates derived from velocity field measurements. In *APS Division of Fluid Dynamics Meeting Abstracts*, 2016.
- [3] T Brockett. Minimum pressure envelopes for modified NACA-66 sections with NACA A= 0.8 camber and buships type 1 and type 2 sections. Technical report, David Taylor Model Basin, 1966.
- [4] David Hanson. *Cavitation Inception for Non-Elliptically Loaded Fins*. Master's thesis, The Pennsylvania State University, 2012.
- [5] Siemens. Star CCM+ v 12.04 User Manual, 2017.

- [6] F. Nicoud and F. Ducros. Subgrid-scale stress modelling based on the square of the velocity gradient tensor. *Flow, Turbulence and Combustion*, 62(3):183–200, 1999.
- [7] Nicholas J Georgiadis, Donald P Rizzetta, and Christer Fureby. Large-Eddy Simulation: Current Capabilities, Recommended Practices, and Future Research. *AIAA Journal*, 48(8):1772–1784, 2010.
- [8] Johan Larsson, Soshi Kawai, Julien Bodart, and Ivan Bermejo-Moreno. Large eddy simulation with modeled wall-stress: recent progress and future directions. *Bulletin of the JSME Mechanical Engineering Reviews*, 3(1), 2016.
- [9] Jim Chow, Greg Zilliac, and Peter Bradshaw. Turbulence Measurements in the Near Field of a Wingtip Vortex. 1997.
- [10] Matthew J Churchfield and Gregory A Blaisdell. Numerical Simulations of a Wingtip Vortex in the Near Field. *Journal of Aircraft*, 46(1):230–243, 2009.